Individual cylinder fuel blend estimation in a dual-fuel engine using an in-cylinder pressure based observer

Carlos Guardiola[a], Benjamín Pla[b], Pau Bares[b], Alvin Barbier[b,*]

[a] *Universitat Politècnica de València, Camino de Vera s/n, E-46022 Valencia, Spain*
[b] *Universitat Politècnica de València, CMT-Motores Térmicos, Camino de Vera s/n, E-46022 Valencia, Spain*

Abstract

Cylinder-to-cylinder combustion dispersion in internal combustion engines might be caused by various factors (e.g. manufacturing variations of the injectors or nozzle coking) which can result in an increase in pollutant emissions. When dealing with low temperature combustion concepts such as premixed dual-fuel, the system might suffer from an additional source of dispersion due to port fuel injection distribution. Conventional cylinder fuel concentration estimation is based on look-up tables previously calibrated and saved in the ECU. The ageing and the fuel distribution characterization of the injectors are a challenging task when relying only on a single UEGO sensor placed at the exhaust. In-cylinder pressure sensors offer a powerful solution to evaluate the energy released by the fuel with one cycle resolution. The present work proposes to combine the information provided by such sensor together with conventional sensors, in this case air mass flow and lambda sensor, for estimating the fuel concentration and blending ratio entering each cylinder in a heavy-duty dual-fuel engine. A Kalman filter was designed to tackle the dynamics of the system, e.g. lambda sensor delay and port fuel distribution, and validated in both conventional diesel and dual-fuel combustion. The output of the filter was then used to update the injectors look-up table in order to cope with ageing and possible bias over time.

Keywords: Dual-fuel combustion, Kalman filter, in-cylinder pressure, heat release calculation, cylinder dispersion, adaptive look-up table

1. Introduction

With the increasingly stringent pollutant emissions regulations for internal combustion engines (ICE), low temperature combustion (LTC) concepts (Agarwal et al., 2017) such as Reactivity Controlled Compression Ignition (RCCI) appeared to be a promising way to emit ultra-low NOx and soot levels while keeping high thermal efficiencies (Kokjohn et al., 2011; Splitter et al., 2013; Benajes et al., 2014, 2017). The RCCI combustion uses a blend of two fuels with different reactivities: a low reactivity fuel (LRF), e.g. gasoline, and a high reactivity fuel (HRF), e.g. diesel. This allows to modulate the fuel mixture reactivity depending on the engine operating conditions and to provide better control of the combustion process compared to other strategies such as Homogeneous Charge Compression Ignition (HCCI) (Reitz and Duraisamy, 2015; Paykani et al., 2016).

From an injection system perspective, common implementation of dual-fuel concepts such as RCCI consists in adding a port fuel injector (PFI) at each intake runner for the LRF while a direct injector (DI) is used for the HRF (Li et al., 2017). In dual-fuel combustion engines, the combustion phasing, usually considered as the crank angle where 50% of the energy contained in the fuel mixture has been released (CA50), is controlled by the in-cylinder reactivity (Hanson et al., 2011; Benajes et al., 2016). Therefore, performance as well as pollutant emissions are sensitive to the operating conditions such as the intake pressure and temperature, the exhaust gas recirculation (EGR) rate, and the injection strategies including the proportion of LRF in the mixture (Benajes et al., 2015; Wang et al., 2016a; DelVescovo et al., 2017). Desantes et al. (2014) reported an improvement of 4% of the gross indicated efficiency maintaining the NOx and soot emissions under EURO VI limits in a single cylinder RCCI engine by setting the proper EGR and gasoline fraction.

In a research environment, cylinder charge composition is estimated thanks to dedicated devices such as fuel balance for the fuel consumption and CO_2 balance technique for the EGR rate using external gas analyzer. However, in on-board applications only a few sensors are available for estimating the in-cylinder mixture. As an example, the injected fuel quantity is usually estimated based on an injector look-up table function of the injector energizing time and a pressure of reference (rail pressure for direct injectors). Nevertheless, over time, the injectors ageing can lead into a different injected fuel mass.

In a multi-cylinder configuration, cylinder-to-cylinder

*Corresponding author
Email addresses: carguaga@upv.es (Carlos Guardiola), benplamo@mot.upv.es (Benjamín Pla), pabamo@mot.upv.es (Pau Bares), albar9@mot.upv.es (Alvin Barbier)

dispersion can represent a source of performance drop and an increase in pollutant emissions. In direct injection engines, small manufacturing variations, ageing, or nozzle coking, might favour the cylinder-to-cylinder air-fuel ratio (AFR) dispersion (Payri et al., 2006a; D'Ambrosio and Ferrari, 2012; Zhang et al., 2020), while in port fuel injection, in addition to the injector bias, AFR dispersion due to the cylinder-to-cylinder air distribution is also expected (Heywood, 1988).

Over the years, different methods were investigated for individual cylinder air-fuel ratio estimation. Universal Exhaust Gas Oxygen (UEGO) sensors placed at the exhaust can provide an air-fuel ratio estimate. Although usually limited to an average engine AFR every cycle (Franceschi et al., 2007; Ebrahimi et al., 2012), some studies aimed to quantify the contribution of each cylinder on the AFR measured by a single UEGO sensor by modeling the exhaust phenomena and dynamics (Chauvin et al., 2006; Suzuki et al., 2007; Cavina et al., 2010; Wang et al., 2019; Guardiola et al., 2019c). In-cylinder pressure can also be used to estimate the composition of the mixture in the cylinder: in Tunestål and Hedrick (2003); Di Leo (2015); Finesso and Spessa (2015), the authors determine the AFR by an inverse combustion model and in-cylinder pressure reading, while in Guardiola et al. (2014); Broatch et al. (2015) investigations suggested to use the resonant frequency of the in-cylinder pressure oscillations to estimate the overall trapped mass. Indeed, Luján et al. (2016) applied this method on HCCI engines showing its potential for diagnosis and control, as these type of engines use to exhibit high resonance excitation (Guardiola et al., 2018b).

Although in-cylinder pressure sensors are not available in all commercial vehicles, they are considered powerful candidates for enhancing the control of low temperature combustion concepts as they provide direct information from the combustion process (Eriksson and Thomasson, 2017; Willems, 2018). In-cylinder pressure sensors are mandatory for a precise estimation of the heat released during combustion, which may be computed in real-time (Asad and Zheng, 2008; Tunestål, 2009). Moreover, the measurement of in-cylinder pressure signal allows the evaluation of the combustion metrics on a per cycle basis, e.g. the indicated mean effective pressure (IMEP), the CA50, or the peak pressure rise rate, which can then be used as a feedback for control strategies based on proportional-integral-derivative (PID) actions (Olsson et al., 2001; Arora and Shahbakhti, 2017; Guardiola et al., 2019a) or to have an insight of the combustion process to develop physical models for model-based controllers (Bidarvatan et al., 2014; Kondipati et al., 2017; Indrajuana et al., 2018; Guardiola et al., 2018a).

The aforementioned works were developed for single fuel applications, however, when dealing with dual-fuel engines, DI injection dispersion is added to PFI variability (Bach et al., 2012; Kassa et al., 2017). As previously mentioned, the portion of LRF injected plays an important role in the combustion control and pollutant formation, a proper estimation of such variable is therefore essential. Some studies can be found for blend ratio (BR) estimation in dual-fuel applications based on different techniques. Most of them are applied to diesel-biodiesel combustion and use either the significant difference in the low heating value (LHV) of both fuels (Beatrice et al., 2011; Junfeng Zhao and Junmin Wang, 2012) or their different oxygen content (Snyder et al., 2010; Mirheidari et al., 2012) to estimate the BR respectively through combustion diagnosis or oxygen concentration measurement at the exhaust. Wang et al. (2015) studied a blending of diesel and gasoline and based their estimation on a multi-factors fusion relying on energy released and ignition delay obtained from in-cylinder pressure measurements. The factors were used to create mean value experimental maps which were then used to estimate the blend ratio for feedforward application. The cylinder-to-cylinder dispersion was however not evaluated.

These type of methodologies might provide valuable information in some operating conditions, but cannot ensure a reliable measurement in all the operating range, henceforth, the information obtained by different sensors and models need to be combined in multi-dimensional scenario, by designing adequate sensor data fusion algorithms (Hasegawa et al., 1994; Moulin et al., 2004; Guardiola et al., 2019b).

The present study investigates the use of the in-cylinder pressure information for estimating the individual cylinder fuel mass amount and blend ratio in a diesel-gasoline multi-cylinder heavy-duty engine. By combining conventional sensors, cycle-to-cycle measurement of the energy released by the fuel mixture, and pre-calibrated look-up tables, the proposed method addresses the cylinder-to-cylinder dispersion, estimates the ratio of both fuels and updates the open-loop (OL) maps in order to improve later control of the engine. Specifically, the proposed method makes use of a Kalman filter to benefit from the available sensors information and to cope with the dynamics of the studied system such as port fuel injection, i.e. wall wetting effect and distribution between cylinders. While state-of-the-art closed-loop control strategies relying on combustion metrics can be effective in single fuel applications for the compensation of the cylinder-to-cylinder dispersion due to fueling variations (Willems et al., 2010), dual-fuel engines represent a more complex environment (Strandh et al., 2004; Willems et al., 2019) especially under diluted operation where similar individual combustion phasing would not necessarily be representative of the same fuel mixture reactivity. The present method might then be used to enhance the feedback information of a dual-fuel combustion closed-loop controller in order to reduce the fuel dispersion between cylinders.

This article is structured as follows: section 2 presents the experimental setup employed, section 3 introduces the models, section 4 investigates the cylinder-to-cylinder fuel dispersion, section 5 and section 6 show the methods and the results obtained respectively, and the last section high-

lights the contribution of this work.

2. Experimental facilities

The experimental data in this study were recorded from a six cylinder heavy-duty diesel engine (see specifications in Table 1) modified to run in both conventional diesel combustion (CDC) and dual-fuel combustion by equipping each cylinder with a port fuel injector.

Table 1: Engine specifications

Bore x Stroke	110 mm x 135 mm
Connecting-rod length	212.5 mm
Compression ratio	12.2:1
Number of cylinders	6
Total displacement	7700 cm^3

The fuels used were commercial gasoline as LRF and diesel as HRF, which low heating values are 42.4 and 42.8 MJ/kg respectively. The diesel was direct injected at a rail pressure P_{rail} controlled by the commercial ECU while the gasoline was port fuel injected at a constant injection pressure of 7 bar. Gasoline and diesel fuel consumption were measured by the respective fuel balances.

The control of the injection settings at each cylinder, namely duration of injection (DOI) and start of injection (SOI), was carried out using dedicated devices connected to an embedded Field Programmable Gate Array (FPGA) chassis from National Instruments (NI 9155). A NI 9752 module was used for cam and crank angle synchronization and the injectors pulses were generated by two NI 9751 and two NI 9758 modules for the direct and the port fuel injection, respectively.

The engine setup included a variable geometry turbine (VGT) for varying the boost pressure, both low pressure (LP) and high pressure (HP) exhaust gases recirculation valves and a back pressure (BP) valve at the exhaust to provide the desired air dilution. The BP valve analog command was set by a PXIe-8135 real-time controller while the LP-EGR valves were connected and controlled by CAN using a PXI-8512 card. The HP-EGR valve and the VGT command were governed by the ECU.

The engine was fully instrumented with air mass flow (MAF), pressure and temperature sensors, and a UEGO sensor was placed close to the turbine outlet (λ_s). Additionally, each cylinder was equipped with an in-cylinder Kistler 6125C pressure sensor (P_{cyl}) and the intake pressure (P_{int}) was measured by a Kistler 4045A10 sensor. Both signals were monitored with a sampling frequency function of the engine speed using a research encoder set with a resolution of 0.2 crank angle degree (CAD) per sample. The acquisition of the different signals was handled by a 16 analog channels acquisition card (PXIe-6358) connected to the real-time controller (PXIe-8135) from National Instruments which was in charge of processing and saving the data. A scheme of the engine control setup is shown in Figure 1 where the blue and grey arrows show the control and the acquisition flow respectively.

The in-cylinder pressure *pegging* (Brunt and Pond, 1997) was done using the intake manifold pressure near the intake bottom dead center (BDC) and the combustion metrics were obtained after filtering the in-cylinder pressure with a low-pass filter tuned at 2.5 kHz.

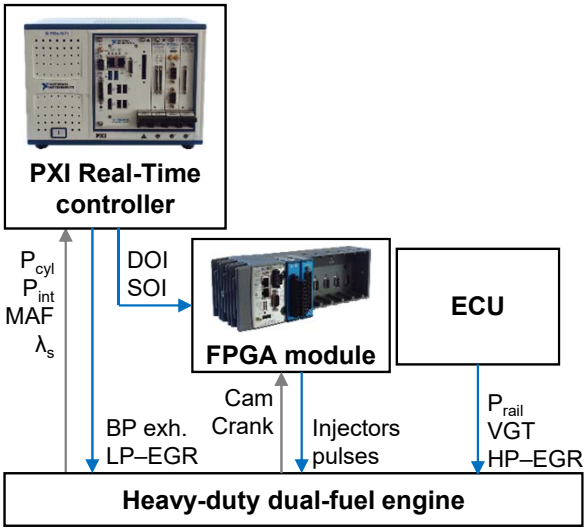

Figure 1: Experimental facilities layout: control actions (blue) and data acquisition (grey)

3. Fuel mass estimation from heat release computation

The energy balance in the cylinder is obtained from the first law of thermodynamics applied to a closed system (thus neglecting injected fuel mass and blow-by) with the ideal gas equation of state:

$$\mathrm{d}Q = \frac{\gamma}{\gamma - 1} p \mathrm{d}V + \frac{1}{\gamma - 1} V \mathrm{d}p \tag{1}$$

where p is the in-cylinder pressure, V the instantaneous volume obtained by geometric crankshaft-piston position, γ the heat capacity ratio, and $\mathrm{d}Q$ represents the heat transferred to the system.

A good approximation for the heat variation in the system ($\mathrm{d}Q$) is described by a source, the heat released by the chemical energy of the combustion of the fuel ($\mathrm{d}Q_c$), and a sink, the heat transferred to the walls ($\mathrm{d}Q_{ht}$), following:

$$\mathrm{d}Q = \mathrm{d}Q_c - \mathrm{d}Q_{ht} \tag{2}$$

The heat capacity ratio γ is dependent on the species concentration and temperature of the system and may thus vary during the engine cycle. In this model it was decided to calculate its value at each crank angle degree using the same approach than the one used in Lapuerta et al. (1999).

First, the gas constant R_c of the in-cylinder gas is estimated using the gas constants and the mass fractions of the species contained in the cylinder, being air (m_a), fuel (m_f) and burnt products (m_b):

$$R_c = \frac{1}{m_{cyl}} \left(R_a m_a + R_f m_f + R_b m_b \right) \tag{3}$$

where m_a, m_f and m_b are the instantaneous mass of each species at each crank angle degree and m_{cyl} is the total in-cylinder trapped mass.

Then, the instantaneous in-cylinder temperature is calculated:

$$T = \frac{pV}{m_{cyl} R_c} \tag{4}$$

which value will be used to determine the specific heat at constant volume c_v of the three considered species using polynomial correlations (Lapuerta et al., 1999) and obtain the global c_v:

$$c_v = \frac{1}{m_{cyl}} \left(c_{v_a} m_a + c_{v_f} m_f + c_{v_b} m_b \right) \tag{5}$$

Therefore, using (3) and (5) the instantaneous γ can be estimated:

$$\gamma = \frac{R_c + c_v}{c_v} \tag{6}$$

The heat transferred to the cylinder walls was modeled using Newton's law of cooling, which is based on the engine speed N (in rpm) for its conversion to the crank angle domain (α), the effective heat transfer area A obtained from the geometry of the cylinder and the piston's position, and the thermal gradient between the system and the environment:

$$\frac{\mathrm{d}Q_{ht}}{\mathrm{d}\alpha} = \frac{h_c A}{6N} (T - T_w) \tag{7}$$

where T_w is the temperature of the cylinder walls and h_c is the heat transfer coefficient which was modeled based on the Woschni correlation (Woschni, 1967; Payri et al., 2006b) using the cylinder bore D, the in-cylinder pressure and temperature (p and T), and the average cylinder gas velocity ω:

$$h_c = 0.013 D^{-0.2} p^{0.8} T^{-0.53} \omega^{0.8} \tag{8}$$

where ω was estimated by:

$$\omega = C_1 S_p + C_2 \frac{V_{dis} T_{ivc}}{p_{ivc} V_{ivc}} (p - p_m) \tag{9}$$

with the mean piston speed S_p, the cylinder conditions at intake valve closure (IVC), the instantaneous in-cylinder pressure p, the motored cylinder pressure p_m, and C_1 and C_2 being two empirical constants (Heywood, 1988).

Combining (2) and (7) it is possible to find the evolution of the energy released by the fuel mixture $\mathrm{d}Q_c$. Finally, for a single fuel, considering the combustion efficiency η_c and the low heating value (LHV) as known, the injected fuel mass m_f and the energy released are related through:

$$m_f = \frac{Q_c}{\eta_c LHV} = \frac{1}{\eta_c LHV} \int_{IVC}^{EVO} \mathrm{d}Q_c d\alpha \tag{10}$$

where IVC and EVO are intake valve closing and exhaust valve opening respectively.

This procedure can be used at each cylinder independently, so providing the system with six measurements of injected fuel mass every cycle.

As introduced in (3), (4) and (5), the calculation of the total energy released by the fuel mixture is dependent on the estimation of the in-cylinder charge m_{cyl}. A common way to estimate the total trapped mass is by applying the speed density method. It is based on the pressure and the temperature at the intake port and uses a pre-calibrated volumetric efficiency map function of the engine speed and the intake pressure (Wang et al., 2016b). However, traditional methodologies do not take into account cylinder-to-cylinder variability at the air distribution, which might be specially critical when high-pressure EGR is used (Maiboom et al., 2009; Payri et al., 2010).

In this study it was decided to use the full potential of the in-cylinder pressure sensor by determining the trapped mass from the in-cylinder pressure resonance (Guardiola et al., 2014; Broatch et al., 2015; Luján et al., 2016). This technique relates the frequency of the first resonant mode (f_{res}) to the cylinder mass following:

$$m_{cyl} = \frac{B_{1,0}^2 \gamma p V}{(f_{res} \pi D)^2} \tag{11}$$

where $B_{1,0}$ is the Bessel constant that characterizes the first resonant mode. The reader is invited to refer to the aforementioned references for more information about this method.

3.1. Sensitivity analysis

Although the heat released offers one measurement per cylinder of the fuel burnt with one cycle resolution, it might suffer from some bias due to unknown parameters that vary with the operating conditions, e.g. combustion efficiency. Considering that most of the critical parameters that disturb the measurement of the fuel burnt will similarly affect the different cylinders, the cylinder-to-cylinder dispersion may be estimated with this method.

Nevertheless, it can be assumed that some differences between the cylinders might exist in the compression ratio r_c because of machining disparity between pistons, in the distribution of the trapped mass and/or masses concentration between cylinders due to hardware design, and in the heat released through the walls due to differences in the wall temperature T_w caused by unequal refrigeration in all the cylinders (inner cylinders are usually at higher temperature). These representative factors were numerically

biased to observe the model deviation from the original levels obtained. Their impact on the calculation of the heat released was evaluated at a 1200 rpm-25% load diesel operating point and the respective biases and results are detailed in Table 2. The relative bias ε_{Q_c} was calculated in percentage by comparing the results of the biased calculation with the original ones.

It must be noticed that in the considered heat release computation model, a bias of 0.2 points in the compression ratio will be translated into a variation in the injected fuel mass estimation below 1%. Similarly, a difference of wall temperature of 30 degrees and a 20% reduction in fresh air would cause an estimation deviation below 1%. Finally, a 10% fluctuation in the bulk temperature (or the trapped mass m_{cyl}) would imply a variation of 3% in the final measurement. The model robustness against these parameters was considered representative of the model accuracy and henceforth, it was assumed to be sufficiently precise for the application presented in this work, that is the cylinder-to-cylinder dispersion evaluation. The temperature of the walls, the compression ratio but also the combustion efficiency were therefore considered the same for all the six cylinders.

Table 2: Sensitivity analysis on the heat release model

Variable	Bias applied	Calculated ε_{Q_c}
r_c	0.2 points	<1%
T_w	30°C	<1%
m_a	20%	<1%
m_{cyl}	10%	∼3%

It must be noted that high pressure EGR was found to be responsible of an unequal distribution of the air charge between cylinders, resulting in a different cylinder species concentration (Payri et al., 2010). However, this effect is expected to not impact the fuel quantity estimation considering that if all the fuel is burnt, the same amount of energy should be measured regardless of the species in the cylinder.

4. Fuel mass dispersion characterization

Main applications of injected fuel mass estimation in conventional engine control unit (ECU) rely on built-in look-up tables using the energizing time of the injector and a pressure difference at the injector nozzle: the rail pressure for direct injection (negligible cylinder pressure), and the intake pressure for port fuel injection (constant injection pressure). However, even when using the same control settings, due to manufacturing variations, each injector could inject a different fuel mass. There have been several works dealing with injector bias (Payri et al., 2006a; D'Ambrosio and Ferrari, 2012; Macian et al., 2006). Hereafter an analysis of the injectors dispersion is shown in order to characterize the bias at DI and PFI injection. The fuel burnt at each cylinder is calculated from the total energy released and a bias percentage at each cylinder (Θ_{cyl} [%]) is calculated by comparing the individual cylinder energy to the mean energy released by the six cylinders:

$$\Theta_{cyl} = \frac{Q_{c,cyl} - \overline{Q_c}}{\overline{Q_c}} \quad \text{with} \quad \overline{Q_c} = \frac{1}{6}\sum_{cyl=1}^{6} Q_{c,cyl} \qquad (12)$$

First, the diesel injector was characterized by performing only CDC. Afterwards, a characterization of the gasoline PFI dispersion between cylinders was studied by performing gasoline steps in dual-fuel mode.

4.1. Direct diesel injection characterization

A complete analysis of the diesel injection bias at the six cylinders was performed by analyzing blocks of 100 consecutive cycles at various double diesel injection settings. In these tests, the rail pressure, the duration of injection (DOI), and the dwell time were varied to analyze their effect on the cylinder-to-cylinder dispersion.

Here, conventional diesel combustion was performed in order to isolate the diesel injectors in the calculation of the energy released. The injection duration and rail pressure levels were chosen according to dual-fuel operation over the whole engine map and the injection timings were adapted to CDC conditions to avoid high pressure rise rate levels.

Figure 2 shows the bias Θ_{cyl} obtained for all six cylinders at various rail pressure values, ranging from 600 to 2000 bar, and for four values of DOI of the main injection, namely 700, 900, 1100 and 1300 μs while keeping the duration of the pilot injection and the start of both injections (SOI) constant at 400 μs, and 15 and 5 CAD before top dead center (bTDC) respectively.

Note that for a given cylinder and DOI, the rail pressure affects the bias: as P_{rail} increases the bias tends to decrease. It can also be seen that increasing the duration of injection tends to decrease the bias for all the cylinders (in percentage).

Figure 3 shows the bias found at each cylinder for various dwell times (from 0.7 to 1.8 ms), which corresponds to the time between the end of the pilot injection and the start of the main injection, at three levels of rail pressure and constant engine speed of 1200 rpm. Here, the start of the pilot injection and the duration of both injections were kept constant at 15 CAD-bTDC, and 400 and 1100 μs respectively, while only the SOI of the main injection was changed. At a constant dwell time and rail pressure, the engine speed might affect the rail dynamics and thus alter the cylinder-to-cylinder fuel distribution. Despite of such statement and the small variations which can be appreciated in Figure 3, in this work the authors assumed that the dwell time does not affect the injection dispersion between cylinders.

As the injection dispersion is supposed to depend only on the DOI and the rail pressure, but not on the operating conditions, one way to take into account the cylinder-

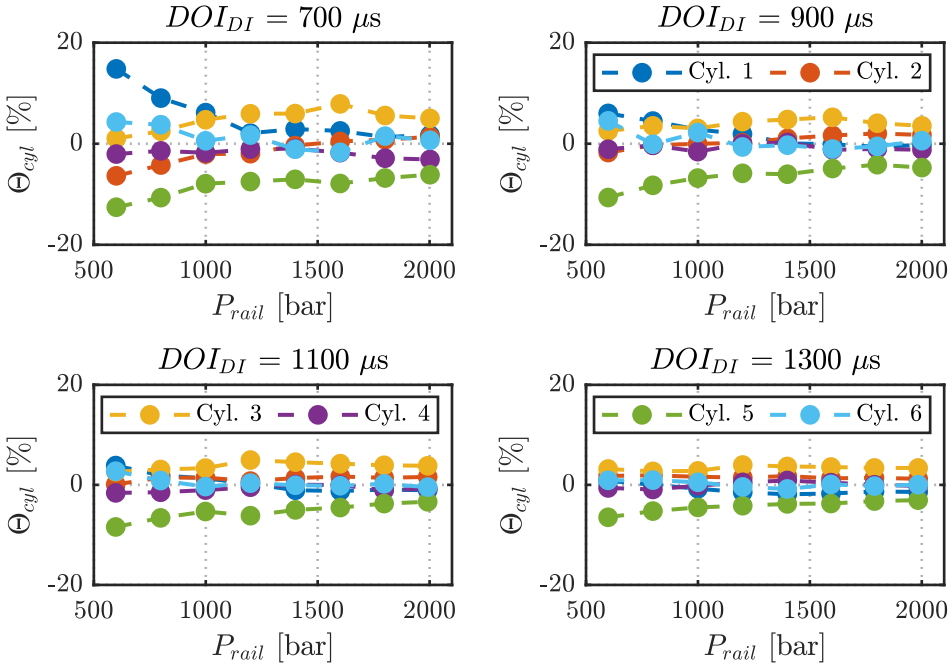

Figure 2: Energy bias percentage at each cylinder at different DOI and rail pressure compared to the mean energy released by all the cylinders

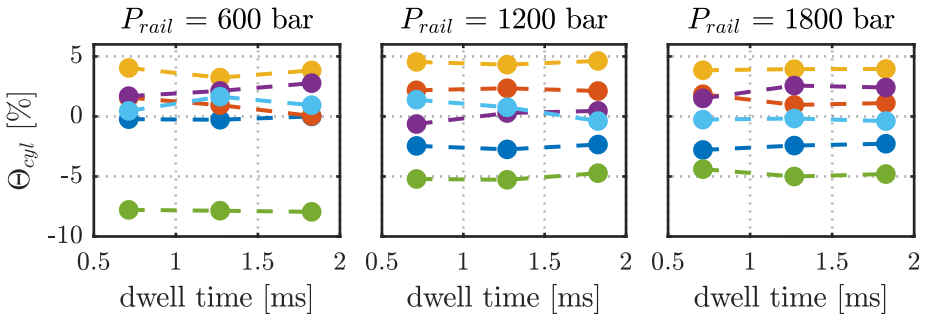

Figure 3: Energy bias percentage at each cylinder at different dwell time and rail pressure compared to the mean energy released by all the cylinders (the reader is referred to Figure 2 for the cylinder color legend description)

to-cylinder dispersion in the control unit is to measure the injection rate at each injector under different injection settings and to obtain which correction should be applied on each injector. Such method is usually performed by car/truck manufacturers when installing the injectors in a new engine. Each injector is firstly tested and then a specific coefficient is applied in the ECU to consider such dispersion. However, phenomena such as coking due to particulate matter produced by the combustion over time can interfere with such calibration.

An analysis of several tests with the same engine during 17 months at the same operating point (1200 rpm and 25% load with same injection settings) was conducted to analyze the evolution of the injectors bias. Figure 4 shows that over time, the bias at each injector is not necessarily constant and might change depending on factors such as the injector's clogging. In this figure, the biases at each cylinder are shown in the top plot. The bottom plot shows the fuel mass estimation from the mean energy of all the six cylinders (with a combustion efficiency assumed to be constant and equal to 0.98) together with the value given by the fuel balance in mg/stroke, where "stroke" refers to "per cycle per cylinder".

It can be observed in the bottom plot that both the fuel balance and the fuel estimation are providing similar fuel quantities. Nevertheless, although the mean fuel mass remains relatively constant, each injector's contribution is shown to vary over time in the top plot. Such variation might be explained by ageing or deposits accumulation, and shows the need to assess each injector individually.

4.2. Port fuel gasoline injection characterization

Similarly to the direct injection, the port fuel injection variability was studied. In the case of such injection

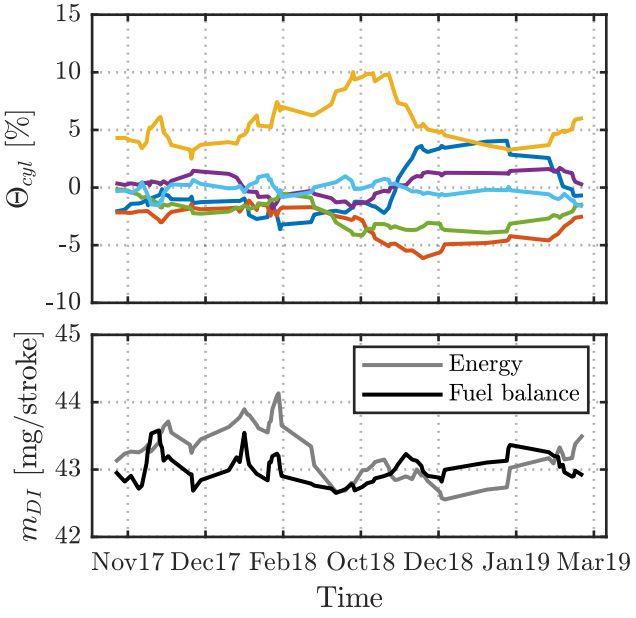

Figure 4: Energy bias at each cylinder at a reference diesel operating point over time (top plot, the reader is referred to Figure 2 for the cylinder color legend description), and estimated fuel mass from energy released in grey and fuel balance measurement in black (bottom plot)

system, due to the intake manifold design, the air flow dynamics, or the port fuel injectors location, some fuel injected from one injector may actually not end up inside of the corresponding cylinder. Figure 5 aims to investigate if such phenomena could be an additional source of cylinder-to-cylinder dispersion. In this test the pilot and the main diesel injections were maintained both in DOI (800 and 920 μs) and SOI (15 and 5 CAD-bTDC) at a constant injection pressure of 600 bar. Here, the duration of the gasoline injection of only one injector was varied from 0 to 3500 μs and the energy released Q_c was calculated in all the cylinders. The amount of energy at each DOI_{PFI} level was then averaged for each cylinder and was analyzed. The procedure was then repeated for each cylinder and the results are listed in Table 3.

Each row of Table 3 represents the cylinder where a change in the DOI was performed and each column shows the variation measured in the energy released at each cylinder. As expected the diagonal matrix, in bold, shows that the highest variation in the energy released Q_c is measured at the cylinder where the DOI is increased. However, it can be observed that some variations are also obtained in other cylinders. As an example, in the case where the change in DOI is applied to cylinder 4, both cylinders 5 and 6 exhibit a significant Q_c variation reaching around 10% of the variation of cylinder 4 in cylinder 5.

Such statement shows that the sources of cylinder-to-cylinder dispersion in such a complex setup can be various and must be considered when developing control strategies applied to dual-fuel engines. Note that the total energy

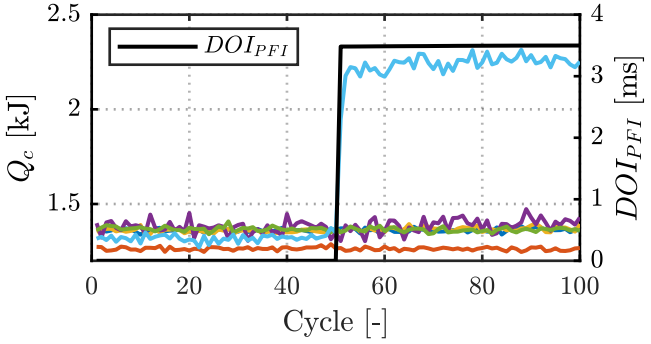

Figure 5: Port fuel DOI variation at a single cylinder for measuring the impact on the energy released by all the cylinders (the reader is referred to Figure 2 for the cylinder color legend description)

Table 3: Results of cylinder-to-cylinder dispersion from PFI variations as shown in Figure 5

ΔDOI	Variation ΔQ_c [J]						
Cyl.	1	2	3	4	5	6	Total
1	**1034**	18	7	25	-3	5	1086
2	25	**902**	16	2	-1	11	955
3	24	33	**887**	26	16	0	986
4	24	8	6	**774**	80	62	954
5	10	-2	7	-34	**900**	26	907
6	1	0	5	-23	-7	**952**	928

variation shown in the last column of Table 3 varies with the cylinders. Excluding the eventual heat release computation errors, this observation might indicate that each injector could be providing a different amount of fuel for the same injection settings due to different conditions at the nozzle, e.g. intake pressure.

It was found that the port fuel injection exhibits a high sensitivity to the air flow dynamics at the intake. Figure 6 shows the cylinder-to-cylinder dispersion when maintaining constant the diesel injection (rail pressure and duration) and varying only the DOI of the gasoline injection starting with no gasoline and up to 4000 μs in all the cylinders, with variation of intake pressure conditions. It can be observed that although having the same injection settings, the bias Θ_{cyl} differs in both amplitude and position depending on the conditions at the intake manifold.

5. Fuel distribution estimation method

In this work it was decided to use a double strategy for the final fuel distribution estimation: (i) the bias caused by the variable operating conditions is estimated by an observer, and (ii) the look-up tables with the injector bias are slowly updated. The aim of the observer is twofold: it uses additional sensors, namely lambda or fuel balance (in test bench applications) to update the combustion efficiency, and it combines the estimation of the overall energy

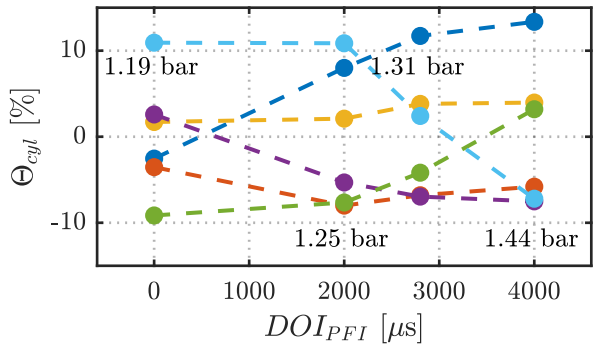

Figure 6: Energy bias percentage at each cylinder in a dual-fuel combustion varying DOI of the port fuel injection. The pressure indication is the intake manifold pressure at each DOI (the reader is referred to Figure 2 for the cylinder color legend description)

delivered by the fuel with the diesel injection to determine the quantity of gasoline in the cylinder.

5.1. Observer design

Following the conclusions of the previous section, it is stated that the bias at each direct injector can be smoothly adapted by the look-up tables by assuming that the in-cylinder conditions do not affect the injection dispersion, and that it is caused by slow dynamics (e.g. ageing, deposits accumulation, etc). Furthermore, in a dual-fuel operation, one of the two injection system needs to be previously calibrated in order to attribute the measured energy difference to the other fuel. Being less prone to external disturbances, the diesel injection was therefore considered as an input of the observer. The estimated diesel bias is considered as an overall one for each injector since the injected fuel mass distribution between pilot and main injection is not addressed here.

Due to the port fuel injection sensitivity to the local conditions around the nozzle, but also to the air distribution that might influence cross injection between cylinders, it was decided to use a single look-up table function of the injection duration and the intake manifold pressure. At every engine cycle k, the look-up table provides a fuel quantity estimation considered the same for all the port fuel injectors. The final gasoline entering each cylinder, however, might be higher or lower than the fuel coming from the injector due to the cross injection (see section 4.2). This phenomena was considered using six states which aim to cope with the gasoline quantity distribution between cylinders such as:

$$\boldsymbol{\theta}^k_{\boldsymbol{PFI}} = \boldsymbol{\theta}^{k-1}_{\boldsymbol{PFI}} \tag{13}$$

Such state is a factor assumed to be constant from one cycle to the other, and is applied to the value provided by the single look-up table. Their product represents the final quantity of gasoline reaching each cylinder intake port (in steady state conditions $\sum \boldsymbol{\theta}_{\boldsymbol{PFI}} = 6$ due to mass conservation). Note that in the equations describing the observer design the bold type is used for multiple cylinder vector notation ($\boldsymbol{\theta} = [\theta_1 \dots \theta_6]^T$).

Additionally, six states were used for the port fuel injection dynamics resulting from the fuel film at the intake walls (Aquino, 1981; Coppin and Maamri, 2010):

$$\boldsymbol{m}^k_{\boldsymbol{ff}} = (1-\beta)\,\boldsymbol{m}^{k-1}_{\boldsymbol{ff}} + (1-\alpha)\,m^{k-1}_{PFI,OL}\,\boldsymbol{\theta}^{k-1}_{\boldsymbol{PFI}} \tag{14}$$

where α and β are calibration constants which, in the case at hand, were assumed to be the same for the six cylinders.

The measured energy released is associated to the injected fuel quantity through the combustion efficiency. The cylinder-to-cylinder dispersion being addressed by the aforementioned states, the combustion efficiency was assumed to have a similar impact in all the cylinders and a single state was therefore considered:

$$\eta^k_c = \eta^{k-1}_c \tag{15}$$

In addition, the lambda sensor can provide an overall fuel quantity estimation with the air flow measurement. It was therefore decided to include this feature in the observer design considering a first order system for the time response of the lambda sensor, e.g. gas transport delay, with the following state:

$$\lambda^k = a\,\lambda^{k-1} + (1-a)\,\frac{1}{\psi_s}\frac{m^{k-1}_a}{m^{k-1}_f} \tag{16}$$

with a the constant characterizing the time response of the sensor and ψ_s the stoichiometric air-to-fuel ratio assumed to be the same for both the fuels used in this study and equal to 14.6. The total injected fuel mass m_f is obtained using the energy released and the diesel mass, assuming that the respective low heating values are known:

$$m^{k-1}_f = \frac{1}{6}\sum\left(\boldsymbol{m}^{k-1}_{\boldsymbol{DI}} + \left[\frac{\frac{\boldsymbol{Q}^{k-1}_{\boldsymbol{c}}}{\eta^{k-1}_c} - \boldsymbol{m}^{k-1}_{\boldsymbol{DI}}\,LHV_{DI}}{LHV_{PFI}}\right]\right) \tag{17}$$

A graphical representation of the respective dynamics from m_{ff} and λ, and their modeling after calibration of the constants α, β and a, can be found in Figure 7.

The measurements of the system consist in the heat released at each cylinder, which is defined by:

$$\boldsymbol{Q}^k_{\boldsymbol{c}} = (\boldsymbol{Q}^k_{\boldsymbol{DI}} + \boldsymbol{Q}^k_{\boldsymbol{PFI}})\,\eta^k_c \tag{18}$$

$$\boldsymbol{Q}^k_{\boldsymbol{DI}} = \boldsymbol{m}^k_{\boldsymbol{DI}}\,LHV_{DI} \tag{19}$$

$$\boldsymbol{Q}^k_{\boldsymbol{PFI}} = (\alpha\,m^k_{PFI,OL}\,\boldsymbol{\theta}^k_{\boldsymbol{PFI}} + \beta\,\boldsymbol{m}^k_{\boldsymbol{ff}})\,LHV_{PFI} \tag{20}$$

and the measurement provided by the lambda sensor λ_s at the exhaust:

$$\lambda^k_s = \lambda^k \tag{21}$$

The state space representation of the system in its discrete form of one cycle step is:

$$x_k = f(x_{k-1}, u_k) + w_k \tag{22}$$

$$y_k = h(x_k, u_k) + v_k \tag{23}$$

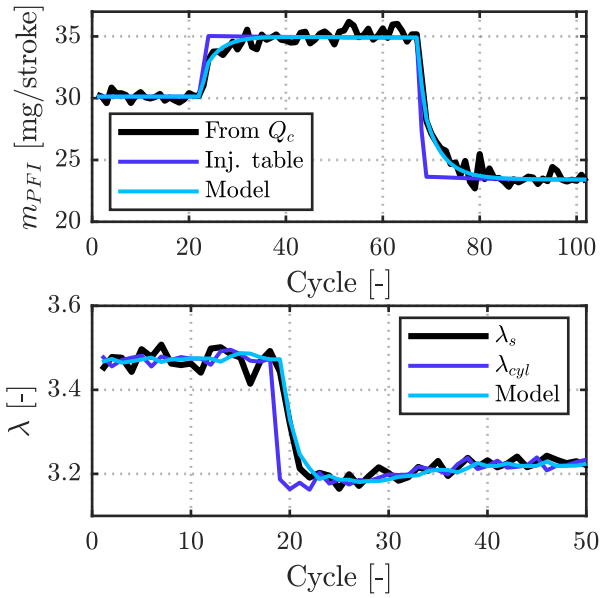

Figure 7: Modeling of the dynamics at the port fuel injection for considering the wall wetting effect (top) and at the λ measurement for gas transport delay (bottom). λ_{cyl} represents the value of lambda estimated from air and fuel mass at every cycle, right part of (16), and λ_s is the value measured by the lambda sensor.

where x are the states, y the outputs, u the inputs, and w and v are the process and observation noises modeled as a Gaussian distribution with zero mean and covariance matrices W and V, respectively.

Henceforth the presented system is composed from the following states x, measurements y, and inputs u:

$$x = \begin{pmatrix} \theta_{PFI,1} \\ \vdots \\ \theta_{PFI,6} \\ m_{ff,1} \\ \vdots \\ m_{ff,6} \\ \eta_c \\ \lambda \end{pmatrix}, y = \begin{pmatrix} Q_{c,1} \\ \vdots \\ Q_{c,6} \\ \lambda_s \end{pmatrix}, u = \begin{pmatrix} m_a \\ m_{DI,1} \\ \vdots \\ m_{DI,6} \\ m_{PFI,OL} \end{pmatrix} \tag{24}$$

In test bench applications, in addition to lambda, the measurement provided by the fuel balances, gasoline and diesel, can be considered by including them in the measurements vector.

A Kalman filter (KF) was chosen to estimate the states of the system described in (24) where the state vector is defined by:

$$\hat{x}_{k|k-1} = f(\hat{x}_{k-1}, u_k) \tag{25}$$
$$e_k = y_k - h(\hat{x}_{k|k-1}, u_k) \tag{26}$$
$$\hat{x}_k = \hat{x}_{k|k-1} + K_k e_k \tag{27}$$

The KF is characterized for minimizing the expected estimation error by solving an iterative Riccati matrix equation and updating the value of the Kalman gain (K), following:

$$P_{k|k-1} = F_k P_{k-1} F_k^T + W_k \tag{28}$$
$$K_k = P_{k|k-1} H_k^T \left(H_k P_{k|k-1} H_k^T + V_k\right)^{-1} \tag{29}$$
$$P_k = (I - K_k H_k) P_{k|k-1} \tag{30}$$

where the covariance matrices W_k and V_k are constant and diagonal, and F_k and H_k are the state transition and observation matrices of the system representing (22) and (23) respectively. In the considered system, these equations are non-linear and an extended Kalman filter (EKF) was therefore used by linearizing them around the current estimate such as:

$$F_k = \left.\frac{\partial f}{\partial x}\right|_{\hat{x}_{k-1}, u_k} \tag{31}$$
$$H_k = \left.\frac{\partial h}{\partial x}\right|_{\hat{x}_{k|k-1}} \tag{32}$$

The Kalman filter outcome is function of its noises calibration in the covariance matrices. A trade-off between observer stability and convergence for the investigated application needs to be found (Blanco-Rodriguez, 2014).

5.2. Adaptive look-up tables

In parallel to the Kalman filter, this work proposes to update the look-up tables dedicated to the injection systems in order to cover eventual bias due to manufacturing discrepancies or ageing over time. Similarly to DI, the single PFI look-up table is updated for coping with eventual bias over time. The strategy is based on a principle which was used in timing control applications for spark ignition engines (Tamaki et al., 2014; Gao et al., 2017). Particularly, it was decided to learn from the value given by the model and update the look-up table utilizing a Gaussian filter in order to adapt the complete grid of the table. Compared to a single grid node update strategy, this method ensures improved smoothness of the complete map and could provide better results when operating in a region which has not been run previously. Each grid node value Z_{ij} is considered part of a map which axes are (X_i,Y_j) with $i = 1, 2, ...n$ and $j = 1, 2, ..., m$ and is calculated as follows:

$$Z_{ij}^k = Z_{ij}^{k-1} + (z_k - \widehat{z}_k) \frac{\Omega(x_k, y_k, X_i, Y_j)}{\Omega(x_k, y_k)} \delta \tag{33}$$

where $(z_k - \widehat{z}_k)$ represents the error between the output of the model and the estimate based on the actual look-up table, and x_k and y_k are here the actual map coordinates of the operating point at cycle k. Here $\Omega(x_k, y_k, X_i, Y_j)$ is the weight factor applied to each grid node of the map and is determined by a Gaussian function resulting from

the distance between the operating point (x_k,y_k) and each grid node:

$$\Omega = \frac{1}{\sqrt{2\pi}\sigma_x} exp\left(-\frac{(x_k - X_i)^2}{2\sigma_x^2}\right) \cdot \frac{1}{\sqrt{2\pi}\sigma_y} exp\left(-\frac{(y_k - Y_j)^2}{2\sigma_y^2}\right) \quad (34)$$

Here, σ_x and σ_y are the standard deviations for each coordinates and act as smoothing factors for the learned-map. Finally, δ in (33) is used as a tuning variable for the fastness of the learning algorithm.

Figure 8 shows the scheme of the combined fuel estimation algorithm. The final estimation is composed from two blocks: a first one, composed from the look-up tables, which are slowly updated, and another one, with the Kalman filter that is able to update the combustion efficiency and the port fuel dispersion in a cycle-by-cycle basis. Note that here the diesel injection is considered as an input of the observer. Therefore, the individual diesel look-up tables can only be updated when the engine is running in pure diesel operation.

6. Results and discussion

Three sets of experimental data were recorded with the engine described in section 2 for the validation of the proposed fuel distribution estimation method (a graphical representation of the operating conditions can be found in Figure 9):

- Test A: this test aims to evaluate the update capability of the adaptive look-up tables method. For this purpose, a conventional diesel combustion case was selected. The test consists in rail pressure sweeps from 600 to 2000 bar at a constant total DOI of 1500 μs and SOI (15 and 5 CAD-bTDC for pilot and main injection respectively) at a constant engine speed of 1200 rpm. The low-pressure EGR and VGT valves position were maintained constant throughout the test.

- Test B: this test aims to simulate an injection fault or leakage. To this end, the port fuel injection duration was increased in only one cylinder (see black dashed line in the middle top plot of Figure 9). Although the duration in cylinder 1 was changed in practice, the system still believed the duration to be equal in all the cylinders in order to appreciate the observer's response to this scenario. The overall objective is to force a cylinder-to-cylinder dispersion to analyze the behaviour of the proposed method against conventional methods such as relying only on the original look-up table. No EGR was performed in this test and the VGT valve position was constant, as well as were the engine speed (1200 rpm), the injection pressure (600 bar) and both DOI (1600 μs) and SOI of the diesel injections (55 and 40 CAD-bTDC for pilot and main injection respectively).

- Test C: this dataset is composed of DOI sweeps in both diesel and gasoline injection. The goal of this test is to show the full ability of the Kalman filter, associated to the adaptive look-up table algorithm, to estimate the fuel distribution between cylinders. The data were collected at a constant engine speed of 1200 rpm and the pilot and the main diesel injections were maintained at constant SOI of 30 and 15 CAD-bTDC respectively. The rail pressure was also kept constant at 600 bar. The VGT and the EGR valve position were maintained unchanged during the test and only low pressure EGR was used in order to ensure a proper mixing and distribution of the charge between the cylinders.

6.1. Test A - Adaptive look-up tables validation

Figure 10 shows the output of the fuel estimation method when applied to Test A (pure diesel case). In particular, the objective is to observe the learning capability of the adaptive look-up table algorithm. The update of the injector model map aims to cope with an eventual deviation over time. This process is slow and the algorithm must be then applied several times to converge to its final state if the starting error is important. The top plot presents the fuel mass estimation from various sources: the original (biased) look-up table, the mean value from the updated look-up tables after the 1^{st} and the 2^{nd} iteration of the test, and the mean energy released by all the cylinders calculated with the heat release model presented in section 3. Note that the purpose of this test is only to give an insight into the adaptive behaviour of the method which works in parallel to the Kalman filter. Consequently, the combustion efficiency was here maintained constant at 0.98 and the lambda measurement, therefore the Kalman filter, was not used in this context. Such assumption might provide an error in the final fuel mass estimation, but is still representative of the cylinder-to-cylinder dispersion and the ability of the algorithm to update the look-up tables.

The speed update of the adaptive look-up tables is controlled by tuning the constant δ_{DI}, see (33), which was here equal to 0.02. In the first iteration, it can be observed that due to an important error at the original look-up tables, the estimated fuel mass exhibits a significant bias. This error is slowly corrected over time to reach the levels given by the measured energy with a mean absolute error of 1.18 mg at the 2^{nd} iteration.

The bottom plot of Figure 10 represents the cylinder-to-cylinder dispersion evaluation through the standard deviation σ of all the cylinders estimations from the different aforementioned methods. In the original look-up table case, such value is constant and equals zero because the same look-up table, which was not updated, was used for all the cylinders. In the case of the 1^{st} and the 2^{nd} iteration

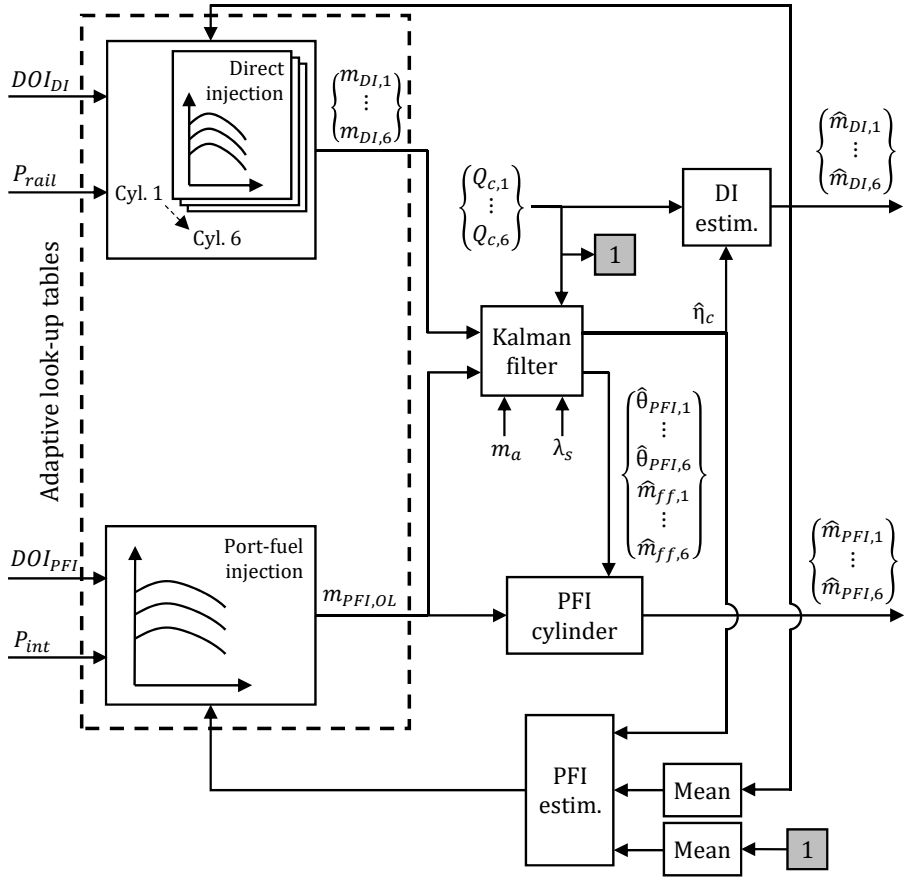

Figure 8: Scheme of the on-board fuel masses estimation method

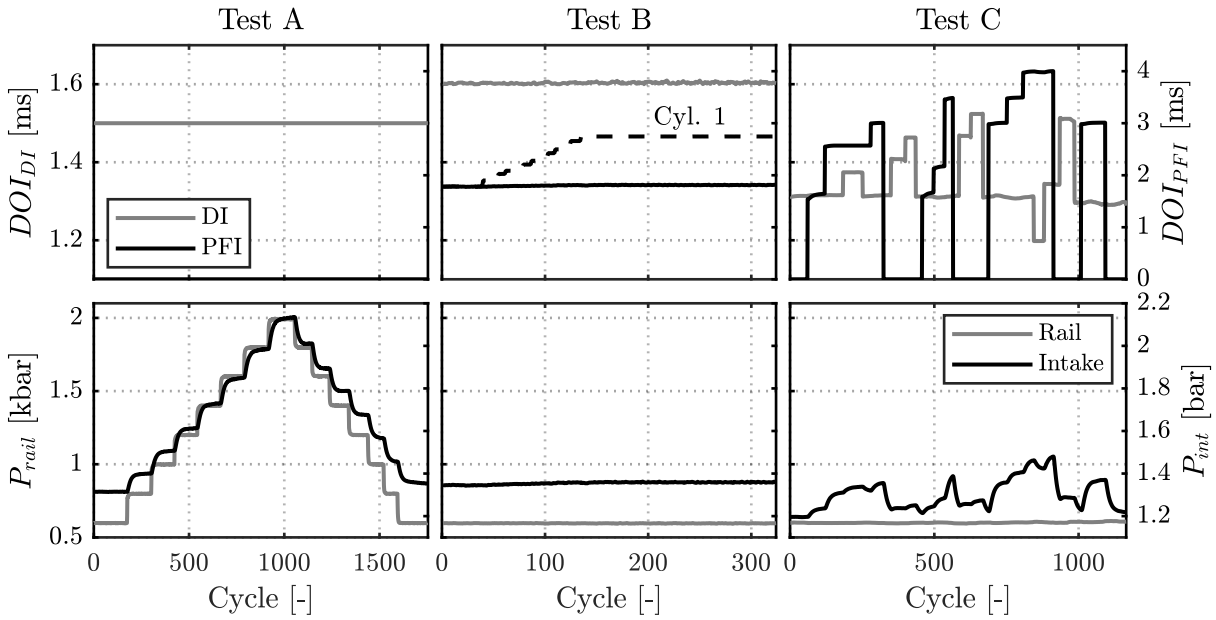

Figure 9: Operating conditions (DOI_{DI}, DOI_{PFI}, P_{rail} and P_{int}) of the experimental data used for the method validation in Test A (left), Test B (middle) and Test C (right)

it can be appreciated that thanks to the individual look-up table correction, the final standard deviation tends to converge to the standard deviation measured at Q_c (represented with black dots). Such observation shows that each injector table is properly updated according to the energy levels obtained at the corresponding cylinder.

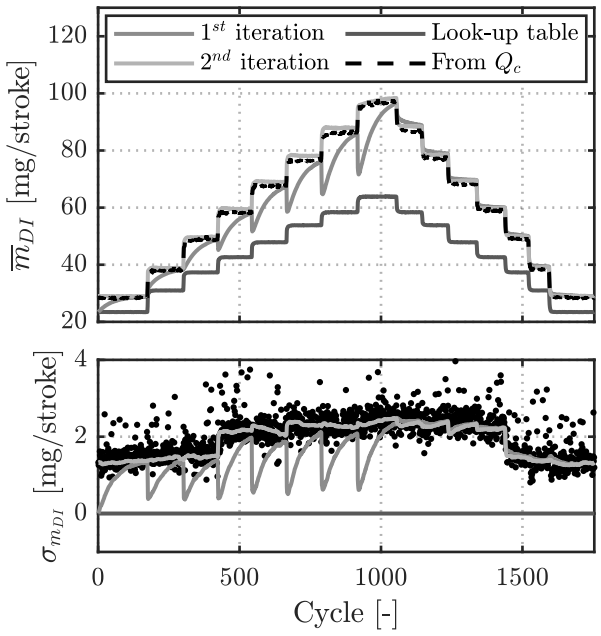

Figure 10: Evaluation of the adaptive look-up tables update applied to Test A. Mean injected fuel mass estimation from various sources (top) and corresponding standard deviation for cylinder-to-cylinder evaluation (bottom)

6.2. Test B - Cylinder-to-cylinder dispersion evaluation from different methods

In Figure 11, the energy levels estimated through various methods are compared in Test B. In this case the diesel quantity was previously calibrated using the fuel balance measurement and considered to be the same in all the cylinders. This might result in a slight starting error in the energy content estimation because the cylinder-to-cylinder dispersion highlighted in section 4 is not addressed but it was considered inconsequential for the goal of this dataset. Indeed, here the objective is to show the ability of the different methods to detect a cylinder-to-cylinder dispersion in the port fuel injection quantity. For this purpose, an important dispersion was intentionally created by increasing the injection duration at cylinder 1 while all the other cylinders were kept constant. However, to fully evaluate the diagnosis ability of each method, it was necessary to simulate the DOI_{PFI} at cylinder 1 as being equal to the other cylinders. By doing so, although the duration is detected as unvarying in the system, in practice the energy released in the cylinder is increased, as this would happen in an injector leakage fault. The studied methods were: (i) relying on the original look-up table only (in grey), (ii) using the look-up table update algorithm for the port fuel injection table (in dark blue), and finally (iii) adding the Kalman filter to the former method (in light blue). The top plot shows the energy content in cylinder 1 estimated by the different methods (the black line is the measured value from the heat release computation), while the bottom plot presents the results obtained at cylinder 2 for comparison purpose.

As expected, it is observed that when the port fuel injection duration in cylinder 1 is increased, the fuel estimation in grey (in other words, the energy content) provided by the original look-up table stays constant which results in an error of around 500 J (∼25%) at the end of the fuel step compared to the measured level (remember that for the look-up table estimation, the duration at cylinder 1 is considered constant and equal to the rest of the cylinders although it is increased in practice, see Figure 9 and description of Test B). Cylinder 2 depicts an error of only 30 J which is justified by the fact that in this case the estimate provided by the look-up table is already closer to the real value. This case highlights the incapacity of the conventional look-up table method to detect any cylinder-to-cylinder dispersion due to the lack of feedback information from the system.

When the update of the port fuel injection look-up table is activated it is noticed that as the PFI content is increased in cylinder 1, the look-up table provides a higher estimate of the injected fuel quantity, resulting in a higher energy released. This is due to the feedback principle in the adaptive look-up table algorithm (see Figure 8). However, by considering a single look-up table for all the port fuel injectors, the final table update can only represent the mean energy released by all the cylinders. Therefore, the energy content of individual cylinders cannot be estimated by a single adaptive look-up table. This is demonstrated by the 20 J reduction in error for cylinder 1, compared to the previous case without the table update error, whilst an error of 480 J still remains at the end of the fuel step. Moreover, in this specific case, this method would even result in a higher error in the case of cylinder 2 (see bottom plot). Likewise the previous method, each cylinder receives the same fuel mass estimation even after the update. As in the conventional diesel Test A, the table update rate is tuned by δ_{PFI} (0.05 in this case).

Finally, in addition to the look-up tables update, the Kalman filter described in section 5 was applied. By doing so, the states participate to the final estimation of the fuel distribution through the energy content in each cylinder. As seen in both plots, this method allows to detect and compensate the energy deviation in cylinder 1 and cylinder 2 with an almost zero mean error after 250 cycles. Using the energy released at each cylinder as a measurement, the fuel distribution between cylinders can be tracked thanks to $\theta_{PFI,cyl}$ while the update algorithm is constantly correcting $m_{PFI,OL}$ (see (18) and Figure 8). Hence, thanks to the use of the KF, both individual cylinder fuel content estimation and cylinder-to-cylinder dispersion can be

addressed compared to the common method relying on look-up tables only.

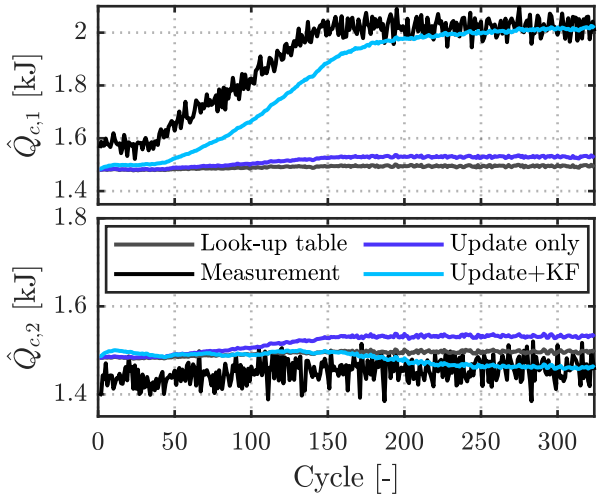

Figure 11: Cylinder-to-cylinder port fuel dispersion detection in Test B from various methods in cylinder 1 (top) and cylinder 2 (bottom)

Table 4: Noises and constants used in the estimation method. The values given for the states and the outputs correspond respectively to the standard deviation of the process and the observation of the Kalman filter ($\sqrt{W}$ and $\sqrt{V}$)

Variable	Type	Equation	Value	Unit
$\theta_{PFI,cyl}$	State	(13)	2e-3	-
$m_{ff,cyl}$	State	(14)	0	mg
η_c	State	(15)	3e-4	-
λ	State	(16)	0.04	-
$Q_{c,cyl}$	Output	(18)	120	J
λ_s	Output	(21)	0.05	-
α	Constant	(14)	0.50	-
β	Constant	(14)	0.25	-
a	Constant	(16)	0.50	-
δ_{DI}	Constant	(33)	0.02	-
δ_{PFI}	Constant	(33)	0.05	-

6.3. Test C - Fuel distribution observer validation

The proposed fuel estimation method was finally applied to Test C which consists in diesel and gasoline DOI sweeps, including both pure diesel and dual-fuel combustion operation. In this case, the Kalman filter together with the look-up tables update are performed and the results can be found in Figure 12. For the sake of clarity this figure shows only a section of the complete test which was previously defined in the right part of Figure 9. The following quantities were chosen to analyze the estimation method output: the standard deviation of the energy released by all the cylinders as an indicator of the cylinder-to-cylinder dispersion evaluation, the energy level at cylinder 1 as an example, and the combustion efficiency and the lambda values for showing the state estimation provided by the Kalman filter. The suggested noises and calibration constants values that were applied for obtaining the results in Figure 12 can be found in Table 4.

Similarly to the previous diesel case in Test A, the method was applied several times on this specific test for evaluating the updating of the injection tables. In the first iteration, errors in the respective diesel and gasoline look-up tables are observed, providing a biased estimate of the energy released (the values from the estimation method are shown in continuous lines while the measurements are in a black dashed line or black dots). Moreover, not only the error at the look-up table could be a reason for explaining the measured energy difference, but also the port fuel distribution between cylinders as concluded in section 4. Therefore, by updating $\theta_{PFI,cyl}$ the cylinder-to-cylinder fuel dispersion is addressed and allows to reduce the error as exhibits the standard deviation plot of the energy released in the top left corner of Figure 12. After the second iteration the individual cylinder fuel concentration and cylinder-to-cylinder dispersion appear to match with the measurements levels. Note that the proposed algorithm updates the diesel look-up tables only under pure diesel conditions. Consequently, if the diesel injection settings are changed during a dual-fuel combustion operation, the eventual error from the diesel injection will be compensated by the gasoline in the Kalman filter and lead to a misestimation of the fuel blend. Nevertheless, the cylinder-to-cylinder dispersion should still be representative.

The combustion efficiency is required to decrease for obtaining similar lambda levels, resulting in a value around 0.91 at the second iteration in that section of Test C. This value is low compared to a conventional threshold observed in CDC (between 0.97 and 0.99). Excluding the effect of the Kalman filter's noises calibration on the estimation, various reasons might be considered to explain such observation: in this study the combustion efficiency is not evaluated using the exhaust gas emissions concentration, e.g. UHC and CO, but represents the energy conversion from the injected fuel. Therefore, the considered fuel low heating values play an important role in the update of such variable, indeed the estimation of the energy released is directly proportional to the LHV, see (18). Also, premixed dual-fuel combustion was found to provide lower combustion efficiencies levels (Kokjohn et al., 2011; Benajes et al., 2014). Finally, the combustion model errors in the energy released estimation might participate in the levels obtained in the present work.

Together with the output of the proposed strategy (1^{st} and 2^{nd} iteration in Figure 12 with Kalman filter and adaptive look-up tables) is shown the results from a simplified method in a dark grey line. In particular, this estimation corresponds to the result of updating only the combustion efficiency to match the lambda level, meaning that the

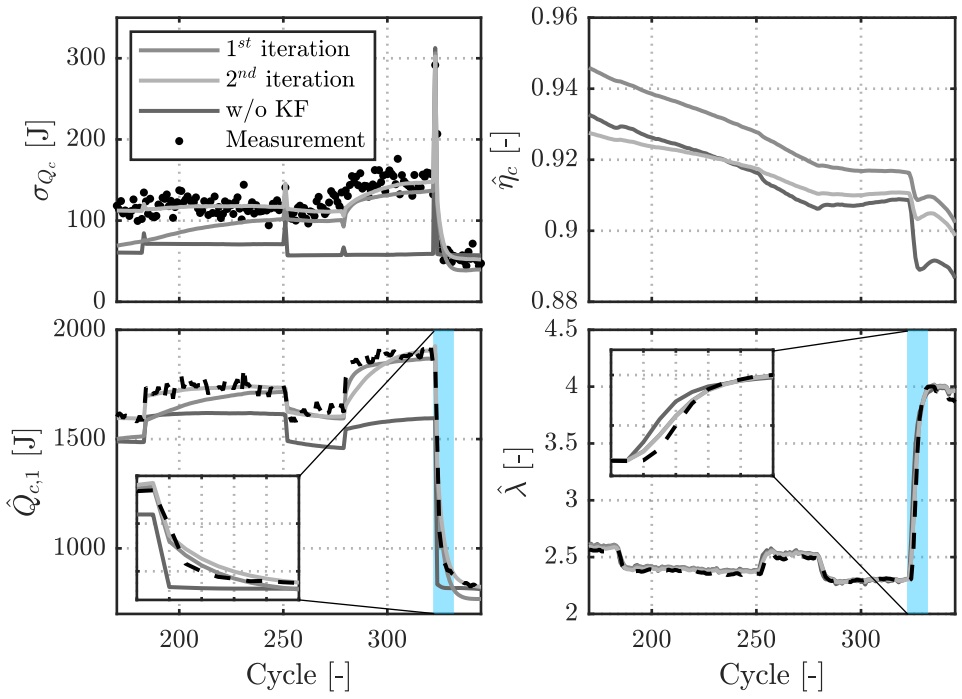

Figure 12: Fuel distribution estimation method applied to Test C. In this figure only a section of the total test is presented showing the standard deviation of the energy released by all the cylinders (top left), the energy content estimated at cylinder 1 (bottom left), the combustion efficiency (top right) and the lambda estimation (bottom right)

port fuel distribution and the dynamics at the fuel film and lambda were not considered. This simplified method aims to show the importance of the different states considered in this study as attest the zoom section in the bottom graphs of Figure 12. Each zoom corresponds to the colored area in their respective graph. It can be observed that thanks to the fuel film mass $m_{ff,cyl}$ in (14) the energy released dynamics when changing the fuel quantities are better captured compared to a straightforward estimation from the look-up tables. Furthermore, the gas transport delay in the lambda measurement in (16) allows to improve its estimation in time which results in a smoother update of the combustion efficiency. Similarly to the conclusions from Test B, it is shown that not considering the fuel distribution by means of $\theta_{PFI,cyl}$ results in an even more inaccurate fuel concentration and distribution estimation.

Figure 13 shows the final estimation of the total injected fuel mass ($m_f = m_{PFI} + m_{DI}$) and gasoline fraction ($GF = m_{PFI}/m_f$) in the complete Test C using the fuel estimation method proposed in this work. Each color represents the individual cylinder fuel estimation after the second iteration, while the black dashed lines represent the levels measured by the fuel balances. It can be noticed that depending on the operating conditions, the cylinder-to-cylinder dispersion is different in both terms of magnitude and order, where the same cylinder does not always provide the same Θ, see (12). Moreover, the trend and the levels achieved by the method show a good agreement with the amounts measured by the fuel balances (note that the fuel balance provides a single value representative of the mean fuel quantity injected in all the cylinders).

Figure 14 aims to analyze the cylinder-to-cylinder dispersion evaluation obtained in Test C. To this end, a section of the test in Figure 13 was selected and the results of cylinder 2 and 4 are compared. Together with m_f and GF, the CA50 is shown as an indicator for the combustion phasing evaluation. In that part of the test, the DOI of the diesel injection is held constant and only the duration of the gasoline injection is increased. An increase in the total fuel mass and in the gasoline fraction is thus expected. Such statement is confirmed in both $\hat{m}_f$ and $\hat{GF}$ graphs.

Around cycle 100, according to the estimation given by the method, the total fuel amount is similar in both cylinders but cylinder 2 exhibits a slightly higher gasoline fraction. This observation may be verified by the CA50 level where cylinder 2 has a later combustion compared to cylinder 4. Indeed, it was observed that an increase in the low reactivity fuel fraction tends to delay the combustion (Hanson et al., 2011; Benajes et al., 2015) as a result of the decrease in the fuel mixture reactivity. This is further observed around cycle 160 where both cylinders are still exhibiting a very similar total fuel amount with a higher gasoline concentration and a more delayed combustion in cylinder 2. The corresponding observations can be further seen in Figure 15 where the heat release rate of these two specific cycles show the lower combustion rate in cylinder 2.

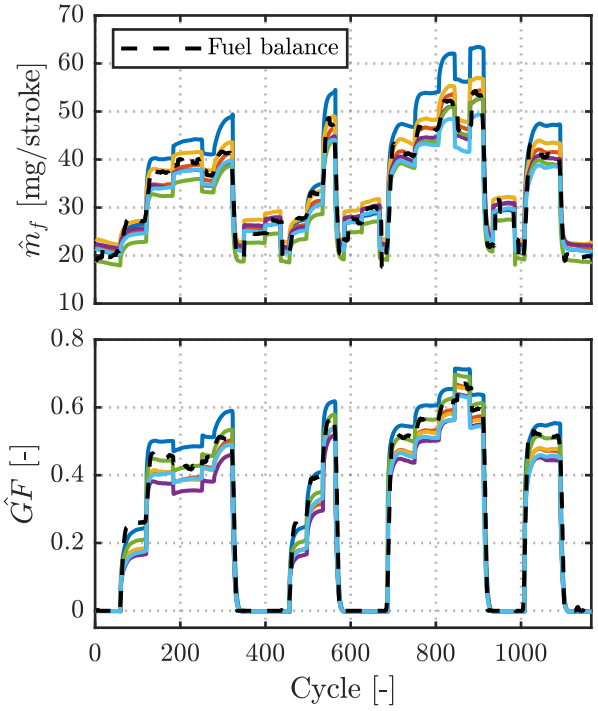

Figure 13: Cylinder fuel concentration (top) and blend ratio (bottom) estimation from the proposed method at the end of the 2^{nd} iteration from Test C (the reader is referred to Figure 2 for the cylinder color legend description)

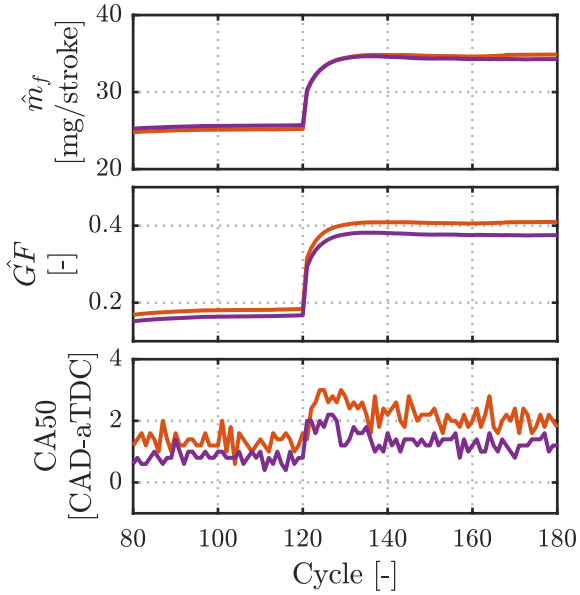

Figure 14: Zoom on a section of the test presented in Figure 13 for studying the dispersion between cylinder 2 (red) and cylinder 4 (purple), aTDC stands for after top dead center

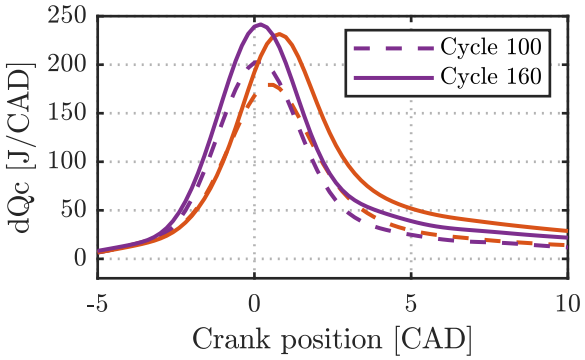

Figure 15: Heat release rate of two specific cycles (100 in dashed line and 160 in continuous line) from Figure 14 for cylinder 2 (red) and cylinder 4 (purple)

7. Summary and conclusion

In this study it was shown that complex hardware configurations such as dual-fuel engines are subject to various sources of cylinder-to-cylinder dispersion, e.g. injector ageing or discrepancies but also port fuel distribution. The present work investigated the use of the in-cylinder pressure signal for individual cylinder fuel mass quantity and blend ratio estimation in a heavy-duty engine modified to run in both conventional diesel and dual-fuel combustion. A model was developed based on the heat release calculation including the heat transfer and proposed to use the resonant components of the cylinder pressure frequencies for the trapped mass estimation. A Kalman filter was then designed to combine the information provided by the set of available sensors and to cope with the system dynamics, e.g. lambda sensor delay and port fuel wall wetting effect. Furthermore, a learning method for updating the individual look-up tables was used to cover injector drift over time using a Gaussian filter to correct the complete grid of the map. The proposed method was applied on three sets of experimental data under different operating conditions.

The first one was used to evaluate the look-up table update algorithm only and exhibited the potential of this feedback method to assess the cylinder-to-cylinder dispersion in conventional diesel combustion. The proposed method relies on the calibration of the diesel injectors look-up tables in order to evaluate the port fuel injection dispersion. This implies that the diesel quantity estimated by the individual tables is considered as an input in the observer and therefore cannot be updated under dual-fuel operation. Nevertheless, if the engine is operated in pure diesel in some areas of the engine map at some point, the DI look-up tables can be updated and therefore address the individual bias over time.

The second experimental dataset consisted in comparing various fuel estimation methods in a dual-fuel combustion. The results highlighted the potential of the Kalman filter to cope with the fuel distribution involved in the port fuel injection system compared to conventional methods relying on look-up tables only.

The last dataset was used to evaluate the full potential of the proposed method in transient conditions switching between CDC and dual-fuel combustion. Individual cylinder fuel amount and fraction were estimated from the outputs of the Kalman filter and the levels obtained exhibited good match with the values provided by the fuel balances. The cylinder-to-cylinder dispersion estimation ability was further observed and verified by heat release analysis.

Such results have shown the importance of considering an injection correction at each cylinder through feedback control for improving performance, engine stability and pollutant emissions in low-temperature combustion concepts such as RCCI. The proposed method was developed for "on-road" application but could be improved by sensor data fusion together with fuel balance measurement and individual UEGO sensor at each cylinder exhaust in a research environment, which would result in a better estimate of the fuel concentration under both steady and transient operation.

8. Acknowledgments

The authors would like to recognize the financial support through Alvin Barbier's grant ACIF/2018/141, *Programa Operativo del Fondo Social Europeo (FSE) de la Comunitat Valenciana 2014-2020*. The authors also wish to thank Gabriel Alcantarilla for his assistance during the experimental campaign.

References

Agarwal, A.K., Singh, A.P., Maurya, R.K., 2017. Evolution, challenges and path forward for low temperature combustion engines. Progress in Energy and Combustion Science 61, 1–56. doi:10.1016/j.pecs.2017.02.001.

Aquino, C., 1981. Transient A/F Control Characteristics of the 5 Liter Central Fuel Injection Engine, in: SAE Technical Paper Series. doi:10.4271/810494.

Arora, J.K., Shahbakhti, M., 2017. Real-Time Closed-Loop Control of a Light-Duty RCCI Engine During Transient Operations. SAE Technical Paper doi:10.4271/2017-01-0767.Copyright.

Asad, U., Zheng, M., 2008. Fast heat release characterization of a diesel engine. International Journal of Thermal Sciences 47, 1688–1700. doi:10.1016/j.ijthermalsci.2008.01.009.

Bach, F., Hampe, C., Wagner, U., Spicher, U., Sauer, C., 2012. Low Temperature Gasoline Combustion With Diesel Micro-Pilot Injection in a Six-Cylinder Heavy Duty Engine, in: ASME 2012 Internal Combustion Engine Division Fall Technical Conference, ASME. p. 349. doi:10.1115/ICEF2012-92127.

Beatrice, C., Guido, C., Napolitano, P., Iorio, S.D., Giacomo, N.D., 2011. Assessment of biodiesel blending detection capability of the on-board diagnostic of the last generation automotive diesel engines. Fuel 90, 2039–2044. doi:10.1016/j.fuel.2011.01.013.

Benajes, J., García, A., Monsalve-Serrano, J., Boronat, V., 2016. Dual-Fuel Combustion for Future Clean and Efficient Compression Ignition Engines. Applied Sciences 7, 36. doi:10.3390/app7010036.

Benajes, J., Garcia, A., Monsalve-Serrano, J., Boronat, V., 2017. Achieving clean and efficient engine operation up to full load by combining optimized RCCI and dual-fuel diesel-gasoline combustion strategies. Energy Conversion and Management 136, 142–151. doi:10.1016/j.enconman.2017.01.010.

Benajes, J., Molina, S., García, A., Belarte, E., Vanvolsem, M., 2014. An investigation on RCCI combustion in a heavy duty diesel engine using in-cylinder blending of diesel and gasoline fuels. Applied Thermal Engineering 63, 66–76. doi:10.1016/j.applthermaleng.2013.10.052.

Benajes, J., Molina, S., García, A., Monsalve-Serrano, J., 2015. Effects of direct injection timing and blending ratio on RCCI combustion with different low reactivity fuels. Energy Conversion and Management 99, 193–209. doi:10.1016/j.enconman.2015.04.046.

Bidarvatan, M., Shahbakhti, M., Jazayeri, S.A., Koch, C.R., 2014. Cycle-to-cycle modeling and sliding mode control of blended-fuel HCCI engine. Control Engineering Practice 24, 79–91. doi:10.1016/j.conengprac.2013.11.008.

Blanco-Rodriguez, D., 2014. Modelling and observation of exhaust gas concentrations for diesel engine control. Springer.

Broatch, A., Guardiola, C., Pla, B., Bares, P., 2015. A direct transform for determining the trapped mass on an internal combustion engine based on the in-cylinder pressure resonance phenomenon. Mechanical Systems and Signal Processing 62, 480–489. doi:10.1016/j.ymssp.2015.02.023.

Brunt, M.F.J., Pond, C.R., 1997. Evaluation of Techniques for Absolute Cylinder Pressure Correction. SAE Technical Paper doi:10.4271/970036.

Cavina, N., Corti, E., Moro, D., 2010. Closed-loop individual cylinder air-fuel ratio control via UEGO signal spectral analysis. Control Engineering Practice 18, 1295–1306. doi:10.1016/j.conengprac.2009.12.002.

Chauvin, J., Petit, N., Rouchon, P., Moulin, P., Corde, G., 2006. Six Degrees Crankshaft Individual Air Fuel Ratio Estimation of Diesel Engines for Cylinder Balancing Purpose, in: SAE Technical Paper Series. doi:10.4271/2006-01-0013.

Coppin, T., Maamri, N., 2010. Fuel estimation and air-to-fuel ratio control for Flexfuel spark-ignition engines, in: 2010 IEEE International Conference on Control Applications, IEEE. pp. 555–560. doi:10.1109/CCA.2010.5611101.

D'Ambrosio, S., Ferrari, A., 2012. Diesel Injector Coking: Optical-Chemical Analysis of Deposits and Influence on Injected Flow-Rate, Fuel Spray and Engine Performance. Journal of Engineering for Gas Turbines and Power 134, 062801. doi:10.1115/1.4005991.

DelVescovo, D., Kokjohn, S., Reitz, R., 2017. The Effects of Charge Preparation, Fuel Stratification, and Premixed Fuel Chemistry on Reactivity Controlled Compression Ignition (RCCI) Combustion. SAE International Journal of Engines 10, 2017–01–0773. doi:10.4271/2017-01-0773.

Desantes, J.M., Benajes, J., García, A., Monsalve-Serrano, J., 2014. The role of the in-cylinder gas temperature and oxygen concentration over low load reactivity controlled compression ignition combustion efficiency. Energy 78, 854–868. doi:10.1016/j.energy.2014.10.080.

Di Leo, R., 2015. Methodologies for air-fuel ratio and trapped mass estimation in diesel engines using the in-cylinder pressure measurement. Energy Procedia 82, 957–964. doi:10.1016/j.egypro.2015.11.850.

Ebrahimi, B., Tafreshi, R., Masudi, H., Franchek, M., Mohammadpour, J., Grigoriadis, K., 2012. A Systematic Air-fuel Ratio Control Strategy for Lean-burn SI Engines. IFAC Proceedings Volumes 45, 296–301. doi:10.3182/20121023-3-FR-4025.00007.

Eriksson, L., Thomasson, A., 2017. Cylinder state estimation from measured cylinder pressure traces - A Survey. IFAC-PapersOnLine 50, 11029–11039. doi:10.1016/j.ifacol.2017.08.2483.

Finesso, R., Spessa, E., 2015. A control-oriented approach to estimate the injected fuel mass on the basis of the measured in-cylinder pressure in multiple injection diesel engines. Energy Conversion and Management 105, 54–70. doi:10.1016/j.enconman.2015.07.053.

Franceschi, E.M., Muske, K.R., Peyton Jones, J.C., Makki, I., 2007.

An Adaptive Delay-Compensated PID Air Fuel Ratio Controller. SAE Technical Paper 2007. doi:10.4271/2007-01-1342.

Gao, J., Zhang, Y., Shen, T., 2017. An On-Board Calibration Scheme for Map-Based Combustion Phase Control of Spark-Ignition Engines. IEEE/ASME Transactions on Mechatronics 22, 1485–1496. doi:10.1109/TMECH.2017.2696788.

Guardiola, C., Pla, B., Bares, P., Barbier, A., 2018a. A combustion phasing control-oriented model applied to an RCCI engine. IFAC-PapersOnLine 51, 119–124. doi:10.1016/j.ifacol.2018.10.022.

Guardiola, C., Pla, B., Bares, P., Barbier, A., 2018b. An analysis of the in-cylinder pressure resonance excitation in internal combustion engines. Applied Energy 228, 1272–1279. doi:10.1016/j.apenergy.2018.06.157.

Guardiola, C., Pla, B., Bares, P., Barbier, A., 2019a. Closed-loop control of a dual-fuel engine working with different combustion modes using in-cylinder pressure feedback. International Journal of Engine Research doi:10.1177/1468087419835327.

Guardiola, C., Pla, B., Bares, P., Stefanopoulou, A., 2019b. Cylinder charge composition observation based on in-cylinder pressure measurement. Measurement: Journal of the International Measurement Confederation 131, 559–568. doi:10.1016/j.measurement.2018.08.024.

Guardiola, C., Pla, B., Blanco-Rodriguez, D., Bares, P., 2014. Cycle by Cycle Trapped Mass Estimation for Diagnosis and Control. SAE Int. J. Engines 7(3), 1523–1531. doi:10.4271/2014-01-1702.

Guardiola, C., Pla, B., Real, M., Travaillard, C., Dambricourt, F., 2019c. Fuel-to-air ratio control under short-circuit conditions through UEGO sensor signal analysis. International Journal of Engine Research , 146808741882074doi:10.1177/1468087418820747.

Hanson, R., Kokjohn, S., Splitter, D., Reitz, R.D., 2011. Fuel Effects on Reactivity Controlled Compression Ignition (RCCI) Combustion at Low Load. SAE International Journal of Engines 4, 394–411. doi:10.4271/2011-01-0361.

Hasegawa, Y., Akazaki, S., Maki, H., Nishimura, Y., Hirota, T., 1994. Individual Cylinder Air-Fuel Ratio Feedback Control Using an Observer. SAE Technical Paper doi:10.4271/940376.

Heywood, J., 1988. Internal Combustion Engine Fundamentals. Automotive technology series, McGraw-Hill.

Indrajuana, A., Bekdemir, C., Feru, E., Willems, F., 2018. Towards Model-Based Control of RCCI-CDF Mode-Switching in Dual Fuel Engines, in: SAE Technical Paper, pp. 1–13. doi:10.4271/2018-01-0263.

Junfeng Zhao, Junmin Wang, 2012. Energy-based and oxygen-based biodiesel blend level estimation methods for diesel engines, in: 2012 American Control Conference (ACC), IEEE. pp. 4975–4980. doi:10.1109/ACC.2012.6314716.

Kassa, M., Hall, C., Ickes, A., Wallner, T., 2017. Modeling and control of fuel distribution in a dual-fuel internal combustion engine leveraging late intake valve closings. International Journal of Engine Research 18, 797–809. doi:10.1177/1468087416674426.

Kokjohn, S.L., Hanson, R.M., Splitter, D.A., Reitz, R.D., 2011. Fuel reactivity controlled compression ignition (RCCI): a pathway to controlled high-efficiency clean combustion. International Journal of Engine Research 12, 209–226. doi:10.1177/1468087411401548.

Kondipati, N.N.T., Arora, J.K., Bidarvatan, M., Shahbakhti, M., 2017. Modeling, design and implementation of a closed-loop combustion controller for an RCCI engine, in: 2017 American Control Conference (ACC), IEEE. pp. 4747–4752. doi:10.23919/ACC.2017.7963689.

Lapuerta, M., Armas, O., Hernández, J., 1999. Diagnosis of DI Diesel combustion from in-cylinder pressure signal by estimation of mean thermodynamic properties of the gas. Applied Thermal Engineering 19, 513–529. doi:10.1016/S1359-4311(98)00075-1, arXiv:9812010v1.

Li, J., Yang, W., Zhou, D., 2017. Review on the management of RCCI engines. Renewable and Sustainable Energy Reviews 69, 65–79. doi:10.1016/j.rser.2016.11.159.

Luján, J.M., Guardiola, C., Pla, B., Bares, P., 2016. Estimation of trapped mass by in-cylinder pressure resonance in HCCI engines. Mechanical Systems and Signal Processing 66-67, 862–874. doi:10.1016/j.ymssp.2015.05.016.

Macian, V., Lujan, J., Guardiola, C., Yuste, P., 2006. DFT-based controller for fuel injection unevenness correction in turbocharged diesel engines. IEEE Transactions on Control Systems Technology 14, 819–827. doi:10.1109/TCST.2006.876924.

Maiboom, A., Tauzia, X., Hétet, J.F., 2009. Influence of EGR unequal distribution from cylinder to cylinder on NOx-PM trade-off of a HSDI automotive Diesel engine. Applied Thermal Engineering 29, 2043–2050. doi:10.1016/j.applthermaleng.2008.10.017.

Mirheidari, S., Franchek, M., Grigoriadis, K., Mohammadpour, J., Wang, Y.Y., Haskara, I., 2012. Real-time and robust estimation of biodiesel blends. Fuel 92, 37–48. doi:10.1016/j.fuel.2011.06.060.

Moulin, P., Corde, G., Castagné, M., Rousseau, G., 2004. Cylinder Individual AFR Estimation based on a Physical Model and using Kalman Filters, in: SAE Technical Paper. doi:10.4271/2004-01-0422.

Olsson, J.o., Tunestål, P., Johansson, B., 2001. Closed-Loop Control of an HCCI Engine. SAE Technical Paper .

Paykani, A., Kakaee, A.H., Rahnama, P., Reitz, R.D., 2016. Progress and recent trends in reactivity-controlled compression ignition engines. International Journal of Engine Research 17, 481–524. doi:10.1177/1468087415593013.

Payri, F., Lujan, J., Climent, H., Pla, B., 2010. Effects of the Intake Charge Distribution in HSDI Engines. SAE Technical Paper Series 1. doi:10.4271/2010-01-1119.

Payri, F., Luján, J.M., Guardiola, C., Rizzoni, G., 2006a. Injection diagnosis through common-rail pressure measurement. Proceedings of the Institution of Mechanical Engineers, Part D: Journal of Automobile Engineering 220, 347–357. doi:10.1243/09544070JAUTO34.

Payri, F., Molina, S., Martín, J., Armas, O., 2006b. Influence of measurement errors and estimated parameters on combustion diagnosis. Applied Thermal Engineering 26, 226–236. doi:10.1016/j.applthermaleng.2005.05.006.

Reitz, R.D., Duraisamy, G., 2015. Review of high efficiency and clean reactivity controlled compression ignition (RCCI) combustion in internal combustion engines. Progress in Energy and Combustion Science 46, 12–71. doi:10.1016/j.pecs.2014.05.003.

Snyder, D.B., Adi, G.H., Bunce, M.P., Satkoski, C.A., Shaver, G.M., 2010. Fuel blend fraction estimation for fuel-flexible combustion control: Uncertainty analysis. Control Engineering Practice 18, 418–432. doi:10.1016/j.conengprac.2010.01.001.

Splitter, D., Wissink, M., DelVescovo, D., Reitz, R.D., 2013. RCCI Engine Operation Towards 60% Thermal Efficiency. SAE Technical Paper Series 1. doi:10.4271/2013-01-0279.

Strandh, P., Bengtsson, J., Johansson, R., Tunestål, P., Johansson, B., 2004. Cycle-to-Cycle Control of a Dual-Fuel HCCI Engine, in: SAE Technical Paper. doi:10.4271/2004-01-0941.

Suzuki, K., Shen, T., Kako, J., Oguri, Y., 2007. Individual A/F control with fuel-gas ratio estimation for multi-cylinder IC engines. Proceedings of the American Control Conference , 5094–5099doi:10.1109/ACC.2007.4282874.

Tamaki, S., Sakayanagi, Y., Sekiguchi, K., Ibuki, T., Tahara, K., Sampei, M., 2014. On-line Feedforward Map Generation for Engine Ignition Timing Control. IFAC Proceedings Volumes 47, 5691–5696. doi:10.3182/20140824-6-ZA-1003.01886.

Tunestål, P., 2009. Self-tuning gross heat release computation for internal combustion engines. Control Engineering Practice 17, 518–524. doi:10.1016/j.conengprac.2008.09.012.

Tunestål, P., Hedrick, J.K., 2003. Cylinder air/fuel ratio estimation using net heat release data. Control Engineering Practice 11, 311–318. doi:10.1016/S0967-0661(02)00045-X.

Wang, J., Yang, F., Ouyang, M., 2015. Dieseline fueled flexible fuel compression ignition engine control based on in-cylinder pressure sensor. Applied Energy 159, 87–96. doi:10.1016/j.apenergy.2015.08.101.

Wang, T., Chang, S., Liu, L., Zhu, J., Xu, Y., 2019. Individual cylinder air–fuel ratio estimation and control for a large-bore gas fuel engine. International Journal of Distributed Sensor Networks 15. doi:10.1177/1550147719833629.

Wang, Y., Yao, M., Li, T., Zhang, W., Zheng, Z., 2016a. A paramet-

ric study for enabling reactivity controlled compression ignition (RCCI) operation in diesel engines at various engine loads. Applied Energy 175, 389–402. doi:10.1016/j.apenergy.2016.04.095.

Wang, Z., Zhu, Q., Prucka, R., 2016b. A Review of Spark-Ignition Engine Air Charge Estimation Methods, in: SAE Technical Papers. doi:10.4271/2016-01-0620.

Willems, F., 2018. Is Cylinder Pressure-Based Control Required to Meet Future HD Legislation? IFAC-PapersOnLine 51, 111–118. doi:10.1016/j.ifacol.2018.10.021.

Willems, F., Doosje, E., Engels, F., Seykens, X., 2010. Cylinder pressure-based control in heavy-duty EGR diesel engines using a virtual heat release and emission sensor. SAE Technical Papers , 1–17doi:10.4271/2010-01-0564, arXiv:2010-01-0564.

Willems, F., Kupper, F., Ramesh, S., Indrajuana, A., Doosje, E., 2019. Coordinated Air-Fuel Path Control in a Diesel-E85 RCCI Engine, in: SAE Technical Paper, pp. 1–11. doi:10.4271/2019-01-1175.

Woschni, G., 1967. A Universally Applicable Equation for the Instantaneous Heat Transfer Coefficient in the Internal Combustion Engine. SAE Technical Paper doi:10.4271/670931.

Zhang, W., Zhang, Z., Ma, X., Awad, O.I., Li, Y., Shuai, S., Xu, H., 2020. Impact of injector tip deposits on gasoline direct injection engine combustion, fuel economy and emissions. Applied Energy 262, 114538. doi:10.1016/j.apenergy.2020.114538.